43rd AIAA Aerospace Sciences Meeting
January 10–13, 2005
Reno, NV

AIAA 2005-0840

A Reduced-Frequency Approach for Calculating Dynamic Derivatives

Scott M. Murman*
ELORET Corp.
MS T27B
Moffett Field, CA 94035
smurman@mail.arc.nasa.gov

Abstract

A novel method of calculating dynamic stability derivatives using Computational Fluid Dynamics is presented. This method uses a non-linear, reduced-frequency approach to simulate the response to a forced oscillation using a single frequency component at the forcing frequency. This provides an order of magnitude improvement in computational efficiency over similar time-dependent schemes without loss of generality. The reduced-frequency approach is implemented with an automated Cartesian mesh scheme. This combination of Cartesian meshing and reduced-frequency solver enables damping derivatives for arbitrary flight condition and geometric complexity to be efficiently and accurately calculated. The method is validated for 3-D reference missile and aircraft dynamic test configurations through the transonic and high-alpha flight regimes. Comparisons with the results of time-dependent simulations are also included.

1 Introduction

Computational Fluid Dynamics (CFD) is increasingly being used to both augment and create an aerodynamic performance database for aircraft configurations. This aerodynamic database contains the response of the aircraft to varying flight conditions and control surface deflections. CFD currently provides an accurate and efficient estimate of the static stability derivatives, as these involve a steady-state simulation about a fixed geometry. The calculation of higher-order dynamic stability derivatives for general configurations and flow

*Senior Research Scientist, Member AIAA

conditions is more costly however, requiring the simulation of an unsteady flow with moving geometry. For this reason the calculation of dynamic stability derivatives using CFD has been limited to either estimating the values at a handful of (hopefully) critical points and extrapolating to cover the range of interest, or using restrictive approximate methods. The need for more efficient, general CFD methods is especially acute as predicting dynamic derivatives with traditional methods, such as wind tunnel testing, is expensive and difficult. As aircraft designs continue to evolve towards highly-maneuverable unmanned systems, high-fidelity aerodynamic databases including dynamic derivatives are required to accurately predict performance and develop stability and control laws. CFD can provide a key technology for modeling the dynamic performance of these advanced systems, with their extreme rate changes and flight conditions.

The current work presents a novel method for calculating dynamic stability derivatives which reduces the computational cost over traditional unsteady CFD approaches by an order of magnitude, while still being applicable to arbitrarily complex geometries over a wide range of flow regimes. Previous approaches can be broadly categorized as general methods which simulate an unsteady motion of the geometry (e.g., a forced oscillation)[1–5], or those which reduce the problem complexity in some manner with an attendant loss of generality. The former methods provide accurate results for arbitrary geometries and flow conditions, however they require a time-dependent moving-body flow simulation, which uses roughly an order of magnitude greater computational time than a static, steady-state simulation. Even predicting one of the roll, pitch, or yaw damping coefficients over the full flight regime is prohibitively expensive. Methods which compute the pitch damping using a lunar coning motion[6–8] can reduce the unsteady, moving-geometry problem to a static, steady-state computation, albeit in a non-inertial reference frame. While these methods provide computational efficiency, they are only applicable to longitudinal damping and require approximating (or ignoring) other damping coefficients. Weinacht[9] extended this approach to predict pitch and yaw damping, however it is only valid for axisymmetric bodies. Weinacht and Sturek[10] demonstrate roll damping calculations in a non-inertial frame for finned projectiles, which also reduces the problem to a steady-state flow solution, however this approach is only valid at $\alpha = 0.0°$. Linearized methods[11, 12] likewise greatly reduce the required computational cost, however, with a loss of accuracy and a reduced range of applicable flow conditions and/or geometric complexity.

A time-dependent simulation supports a continuum of frequencies up to the limits of the spatial and temporal resolution. The primary thesis of this work is that the response to a forced motion can often be represented with a small, predictable number of frequency components without loss of accuracy. By resolving only those frequencies of interest, the computational effort is significantly reduced so that the routine calculation of dynamic derivatives becomes practical. Such "reduced-frequency methods" have recently been extended to retain the non-linearity of the original governing equations by Hall et al.[13, 14] for application to 2-D turbomachinery cascades. McMullen et al.[15, 16] followed this work, also focusing on 2-D turbomachinery flows. The current implementation uses this same non-linear, frequency-domain approach and extends the application to the 3-D Euler equations.

The current work uses a Cartesian, embedded-boundary method[17] to automate the

generation of dynamic stability derivatives. The Cartesian method provides an efficient and robust mesh generation capability which can handle an arbitrarily-complex geometry description. A quality water-tight surface triangulation required for Cartesian mesh generation can be obtained directly from a CAD representation of the geometry[18]. This, combined with the Cartesian embedded-boundary method provides a robust and automatic mesh generation infrastructure which can be utilized through the design process. This meshing scheme has recently been combined with a parallel, multi-level scheme for solving time-dependent, moving-geometry problems, including a generalized rigid-domain motion capability[19]. This Arbitrary Langrangian-Eulerian (ALE) rigid-domain motion scheme provides the foundation upon which the current reduced-frequency method is implemented. The Cartesian methodology has been demonstrated as an efficient, robust method for automatically generating static stability derivatives[20, 21], and the current work extends this to include the prediction of dynamic derivatives.

This paper begins with a brief review of dynamic stability derivatives (Sec. 2), followed by a description of the reduced-frequency approach and implementation (Sec. 3). Section 4 presents the results of several validation cases using reference dynamic test configurations for both missile and aircraft geometries. These validation cases include examples of pitch, yaw, and roll damping calculations using the reduced-frequency method, through both transonic and high-angle-of-attack flight regimes. The computed results are compared against wind-tunnel and ballistic-range data, as well as results computed using a time-dependent method. A detailed cost comparison of the reduced-frequency method is also included. Lastly, the main results of this work are summarized and a choice of future research topics is presented.

2 Dynamic Derivatives

The aerodynamic characteristics of an aircraft can be described by the force and moment coefficients about the body axes; the axial, normal, and lateral force coefficients (C_A, C_N, C_Y), and the roll, pitch, and yaw moment coefficients (C_l, C_m, C_n). In most cases it is sufficient to define these coefficients as functions solely of the flight conditions and aircraft configuration,

$$C_j = C_j \left(\alpha, \beta, M_\infty, h, \delta_i, p, q, r, \dot{\alpha}, \dot{\beta} \right) \tag{1}$$

where j represents each of the individual force and moment coefficients, h is the altitude, δ_i represents any configuration-dependent information such as control surface settings, and p,q, and r are the rotation rates about the body axes.* Each individual coefficient can be broken into two parts: a so-called static portion (subscript s) which depends only on the non-rotating parameters, and a dynamic portion (subscript d) which depends on both the rotational and non-rotating parameters.

$$C_j = C_{j_s} \left(\alpha, \beta, M_\infty, h, \delta_i \right) + C_{j_d} \left(\alpha, \beta, M_\infty, h, \delta_i, p, q, r, \dot{\alpha}, \dot{\beta} \right) \tag{2}$$

*It is assumed that the rotation rates are suitably non-dimensionalized.

The focus of the current work is a method of calculating both the static and dynamic portion of the force and moment coefficients concurrently.

In general the aerodynamic coefficients are non-linear functions of all of the independent parameters, however, in many cases this can be simplified so that a linear superposition of the individual effects of each parameter can be assumed, i.e.

$$C_{j_d} = C_{j_d}(\alpha, \beta, M_\infty, h, \delta_i, p) + C_{j_d}(\alpha, \beta, M_\infty, h, \delta_i, q) + \dots \tag{3}$$

Further, each individual effect is assumed to be due to a linear variation of that parameter, for example the roll variation is given by

$$C_{j_d}(\alpha, \beta, M_\infty, h, \delta_i, p) = C_{j_o}(\alpha, \beta, M_\infty, h, \delta_i) + \frac{\partial C_{j_d}}{\partial p}(\alpha, \beta, M_\infty, h, \delta_i)\,\Delta p \tag{4}$$

Notice that these dynamic derivatives are solely functions of the non-rotating parameters, similar to the static coefficients. In this example, the roll damping derivative is commonly referred to as $\partial C_l/\partial p \equiv C_{l_p}$, with similar notation for the other axes and rates. In many cases the base state coefficients C_{j_o} are equivalent to the static aerodynamic coefficients, C_{j_s}.

Experimentally, the two tools which are commonly used to provide dynamic data are the rotary-balance and forced-oscillation tests. While it is difficult to determine each of the individual dynamic derivatives in the general case, as the rotation about the body and wind axes are coupled, there is a large legacy of methodology for using data from these tests in linearized dynamic models such as described above (cf. Kalviste[22]). The initial focus of the current work is to simulate forced-oscillation testing using a reduced-frequency method, so that the results can be used directly within existing modeling procedures. This is seen as a necessary first step; before more complicated uses for CFD are entertained it must become an everyday tool for evaluating dynamic effects in the most common cases, similar to the manner it is currently being used to evaluate the static effects. A longer-term focus is to develop CFD methods which can compute the dynamic derivatives directly in the general case, and to extend the methods to provide efficient tools in non-linear flight regimes where the traditional methods begin to fail, and obtaining data is extremely difficult (cf. Refs. [23, 24]).

3 Reduced-Frequency Method

The reduced-frequency method is derived from a general time-dependent scheme. An ALE rigid-domain motion approach is used in the current application to simulate a forced motion. The details of this time-dependent ALE scheme with a Cartesian embedded-boundary method are provided in [19], and a brief overview is given here. The time-dependent equations are

$$\frac{\partial \mathbf{Q}}{\partial t} + \mathbf{R}(\mathbf{Q}) = 0 \tag{5}$$

where t is the physical time, $\mathbf{Q}$ is the vector of conserved variables, and $\mathbf{R}(\mathbf{Q})$ is an appropriate numerical quadrature of the flux divergence, $\frac{1}{V}\oint_S \mathbf{f}\cdot\mathbf{n}dS$. This work uses an inviscid

flux vector

$$\mathbf{f} \cdot \mathbf{n} = \left\{ \begin{array}{c} \rho u_n \\ \rho u_n \mathbf{u} + p\mathbf{n} \\ \rho u_n e + p\mathbf{u} \cdot \mathbf{n} \end{array} \right\} \tag{6}$$

where

$$u_n = (\mathbf{u} - \mathbf{u}_\Omega) \cdot \mathbf{n}$$

is the velocity relative to the moving boundary, and $\mathbf{u}_\Omega$ is the velocity of the moving domain.

Following Hall et al. [13, 14], both the conservative variables and $\mathbf{R}(\mathbf{Q})$ are assumed to be periodic functions of time (with frequency ω), and approximated with a finite Fourier series

$$\mathbf{Q}(\mathbf{x}, n\Delta t) \approx \sum_{k=-(N-1)/2}^{(N-1)/2} \hat{\mathbf{Q}}_k(\mathbf{x})\, e^{ik\omega n\Delta t}$$

$$\mathbf{R}(\mathbf{Q}, n\Delta t) \approx \sum_{k=-(N-1)/2}^{(N-1)/2} \hat{\mathbf{R}}_k(\mathbf{Q})\, e^{ik\omega n\Delta t}$$

where $\hat{\mathbf{Q}}_k$ and $\hat{\mathbf{R}}_k$ are complex Fourier coefficients, and $i = \sqrt{-1}$. As a result of this approximation $\mathbf{Q}$ can now only support a reduced set of frequencies, namely ω and the harmonics of ω. Since $\mathbf{R}$ is a non-linear function of $\mathbf{Q}$, the Fourier coefficients $\hat{\mathbf{R}}$ remain a function of $\mathbf{Q}$. Also, since $\mathbf{Q}$ and $\mathbf{R}$ are real, the Fourier coefficients of the negative wavenumbers are complex conjugates of their corresponding positive wavenumber.

The sampling rate Δt is chosen so that the functions are periodic over N samples, i.e. $\omega = \frac{2\pi}{N\Delta t}$ where $T = N\Delta t$ is the period. The Fourier coefficients are thus evaluated using standard Fast Fourier Transform (FFT) algorithms. Substitution of the Fourier expansions for $\mathbf{Q}$ and $\mathbf{R}$ into the time-dependent equation, Eq. 5, gives

$$ik\omega\hat{\mathbf{Q}}_k + \hat{\mathbf{R}}_k(\mathbf{Q}) = 0 \tag{7}$$

which form a set of N independent equations due to the orthogonality of the Fourier modes.* The solution procedure involves first performing an inverse Fourier transform to construct the N samples of $\mathbf{Q}$ from $\hat{\mathbf{Q}}_k$. These samples are used to construct N samples of $\mathbf{R}(\mathbf{Q})$, which are then transformed into the Fourier coefficients $\hat{\mathbf{R}}_k$. Equation 7 is then iterated to convergence by adding a pseudo-time derivative $d\hat{\mathbf{Q}}_k/d\tau$. The source terms that appear in the discretization of Eq. 7 are treated semi-implicitly so that the same CFL condition used for the static, steady-state flow solver can be utilized for the pseudo-time advance of the frequency-domain components.

The reduced-frequency approach outlined above has several convenient features. First, it can be applied to any set of time-dependent equations – inviscid, viscous, Reynolds-averaged turbulence model, etc. – without requiring any special procedures other than a discrete Fourier transform. The same non-linear operator $\mathbf{R}(\mathbf{Q})$ from the time-dependent scheme is

*N independent equations for the real and imaginary parts of the positive wavenumbers. The equations for the complex conjugate are redundant.

computed. Secondly, the same convergence acceleration procedures that are common with static, steady-state solvers, such as local timestepping, multigrid, etc., can be utilized to solve Eq. 7. In the current work all of the existing infrastructure from the parallel, multi-level Cartesian solver developed for steady-state[25], and unsteady dual-time schemes[19] has been re-used in the frequency-domain solver with only minor modifications.

The current approach involves simulating the response to a prescribed periodic motion using an invsicid scheme. The simulations of the base state for these flowfields (steady-state simulations without a prescribed motion) usually result in a time-invariant flowfield, so that all of the unsteadiness in a forced oscillation simulation is due to the prescribed motion. The first mode of $\mathbf{Q}(t)$ is thus identical to the forcing frequency. Further, in an inviscid simulation numerical dissipation is the only mechanism to transfer energy between modes. The numerical dissipation is much less effective than physical kinematic viscosity or turbulence, so that nearly all of the energy remains in the primary mode. Thus, the response to a forced oscillation computed using just a single mode with the reduced-frequency method is often equivalent to a full time-dependent simulation for an inviscid scheme.* This is seen in Fig. 1, which shows the results of simulating the forced oscillation of a transonic NACA 0012 airfoil using three methods: a time-dependent simulation, and reduced-frequency simulations retaining one and two modes. After the initial transient of the time-dependent simulation, all three simulations are nearly identical, and all are in good agreement with the experimental data, capturing the hysteresis in the normal force variation. This indicates that $\mathbf{Q}$ contains just a single mode at the forcing frequency, and that including higher harmonics provides no additional information.

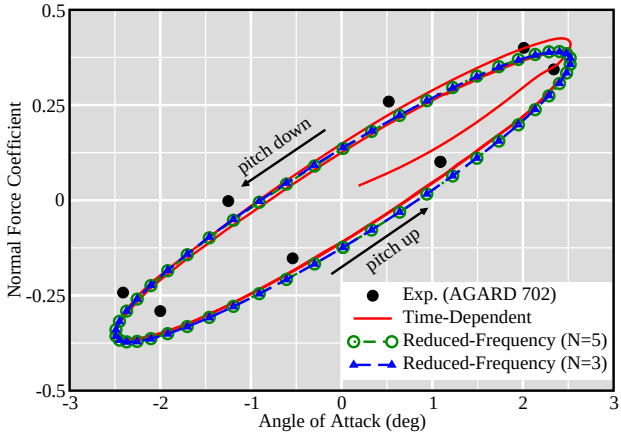

Figure 1: Variation of normal force coefficient with angle of attack for oscillating NACA 0012. ($M_\infty = 0.755$, $\alpha(t) = 0.016 + 2.51\sin(\omega t)$). The time-dependent simulation includes the initial transient portion of the calculation. Experimental data from [26]. The reduced-frequency calculations include one (N = 3) and two (N = 5) frequency components.

The cost of the reduced-frequency approach scales as roughly N times the cost of a static, steady-state solution, as each iteration requires N evaluations of $\mathbf{R}(\mathbf{Q})$. Further, it is required to store N copies of each variable in the scheme, which can be prohibitive in 3-D, especially using commodity desktop systems. Thus, if it requires more than one or two Fourier modes to characterize the unsteady behavior, the reduced-frequency approach rapidly loses favor relative to solving the time-dependent equations, which require roughly an order of magnitude greater effort than a steady-state simulation, but can support a continuum of modes. A comparison of numerical timings for the reduced-frequency and time-dependent methods are presented for 3-D simulations of a forced oscillation in the next section.

*This does not imply that a viscous simulation automatically would show a wide energy band, or that these higher modes must be resolved to provide an effective estimate of the response to a forced oscillation.

As the oscillating NACA 0012 airfoil example demonstrates, simulating a forced oscillation overcomes the two major drawbacks of the reduced-frequency method: the frequency response can be predicted a priori, greatly simplifying the solution procedure; and the response can be accurately modeled using solely the primary frequency mode, leading to a large gain in efficiency which offsets the loss of generality. These features are naturally exploited in the examples in the next section to efficiently calculate dynamic stability derivatives using a forced-oscillation motion.

4 Numerical Results

The calculation of dynamic damping derivatives using the reduced-frequency method outlined above is demonstrated for both missile and aircraft configurations. First, the basics of the method are outlined with the calculation of pitch damping for the Basic Finner missile configuration, including an accounting of the computational cost. Next, damping derivatives are computed for the Modified Basic Finner missile and the Standard Dynamic Model (SDM) aircraft. These examples demonstrate the ability of the method to accurately compute dynamic derivatives through the non-linear transonic and high-alpha regimes. Each of these three configurations are established dynamic experimental test cases with a legacy of both wind-tunnel (forced-oscillation and rotary-balance) and ballistic-range data. This tunnel and range data is used to validate the reduced-frequency method for calculating dynamic derivatives. A mesh refinement study was performed for each computed configuration using the static, steady-state flow solver at nominal flight conditions.

4.1 Basic Finner Missile

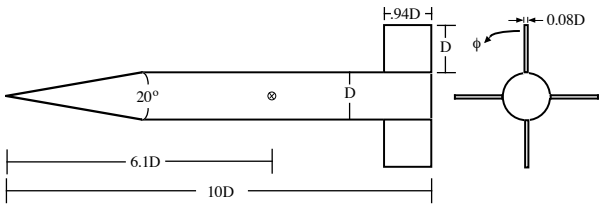

Figure 2: Basic Finner geometry is a cone-cylinder fuselage with square fins in the + configuration. The cone section has a 10° half-angle, and the center of mass is located 6.1 diameters from the nose along the longitudinal axis of the body.

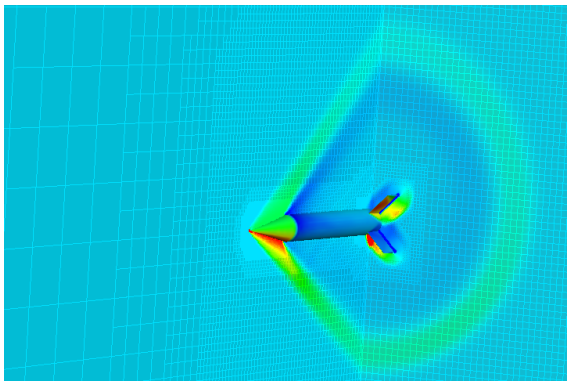

Figure 3: Cutting-plane through the mesh and sample pressure contours for the Basic Finner. Pre-specified mesh adaptation regions were placed around the nose and tail regions, along with an outer box to capture the shock wave emanating from the nose. The mesh contains 500k cells. ($M_\infty = 1.96$, $\alpha = 5°$, $\phi = 45°$).

The Basic Finner configuration is a cone-cylinder fuselage with four square tail fins (cf. Fig. 2). A cutting-plane through the mesh and a sample of the pressure contours around the body from a static, steady-state simulation are presented in Fig. 3. The mesh contains approximately 500k cells. Calculation of the pitch damping at $M_\infty = 1.96$ and angles of attack $\alpha = 0^\circ - 20^\circ$ demonstrates the utility and efficiency of the reduced-frequency method for calculating dynamic stability derivatives. The body is forced to oscillate with a simple sinusoidal function, $\alpha(t) = \alpha_o + \alpha_m \sin(\omega t)$, where all parameters are suitably non-dimensionalized, and α_o is the target angle of attack. The reduced-frequency method with a single frequency mode ($N = 3$) is used to compute the response of the configuration to the forced oscillation.

The DC component computed with the reduced-frequency method provides another approximation for the static, steady-state flowfield. In the forced-oscillation technique the DC component is equivalent to the base state for the dynamic derivatives in Eq. 4. The reduced-frequency method is thus not intended to simply augment static calculations, but rather to *replace* the static, steady-state flow solver for flight and configuration conditions where dynamic information is desired. With a single reduced-frequency calculation both static and dynamic derivative information is obtained. The computational cost of the reduced-frequency method using a single frequency component is presented in Table 1. Rather than present direct CPU timings, which are machine-dependent, the cost is presented relative to the cost of a static, steady-state flow solution. The reduced-frequency method scales as roughly N times the cost of a static, steady-state flow solution, with some overhead for the FFT calculations. There is also a 10-25% overhead with the reduced-frequency method as the ALE residual operator $\mathbf{R}(\mathbf{Q})$ is used, as opposed to the operator from the static flow solver. The ALE scheme uses a general moving-body algorithm, rather than the simpler static Cartesian scheme. The computational cost for a general time-dependent method for computing the dynamic derivatives is also presented for comparison. The time-dependent accounting assumes 100 timesteps/cycle with a 2nd-order time-integration scheme, and an additional 25 timesteps to compute the transient portion of the response. Each timestep requires 15-25 multigrid cycles to converge 2-3 orders of magnitude using the dual-time algorithm with an explicit Runge-Kutta inner loop. The reduced-frequency method provides up to an order of magnitude improvement in computational efficiency over the time-dependent method without loss of generality. A complete set of damping derivatives can be calculated for a fraction of the cost of a single time-dependent moving-body calculation.

Method	Single Axis	Complete Set
Static	1	1
Reduced-Frequency	3.5 - 4	11 - 12
Time-Dependent	25 - 40	71 - 118

Table 1: Computational cost of the reduced-frequency and time-dependent methods for calculating both static and dynamic derivative information at a single flight condition. All values are scaled relative to a single static, steady-state calculation.

Figure 4 presents the convergence of the density residual for the reduced-frequency calculation about the Basic Finner at $M_\infty = 1.96$, $\alpha = 0.0^\circ$ using the multigrid scheme and start-

up procedure. The DC component converges approximately 3 orders of magnitude, while the real and imaginary parts of the frequency component converge 1.5 - 2 orders of magnitude. The frequency components are all initialized to zero. The calculations in this work all use a piecewise linear spatial reconstruction along with the gradient-limiter formulation outlined in Berger et al.[27]. In a sense, the convergence of the reduced-frequency scheme is limited by the convergence of the static, steady-state problem. When convergence of the DC component stalls, the convergence of the frequency components must stall as well, since all of the components are coupled through the temporal-frequency reconstruction/deconstruction process of the method.

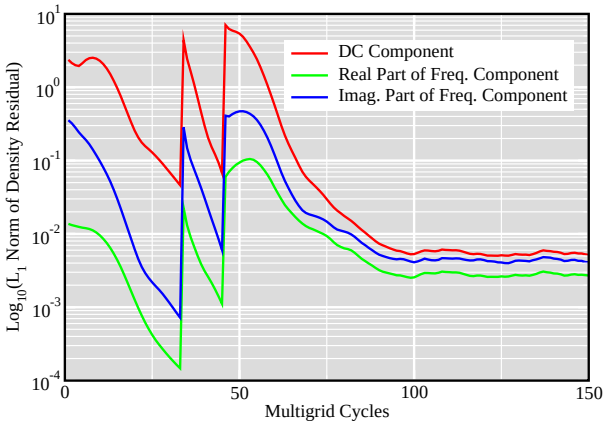

Figure 4: Convergence of the reduced-frequency method for the Basic Finner oscillating in pitch ($M_\infty = 1.96$, $\alpha = 0°$, $\phi = 45°$).

The variation with angle of attack of the static pitching moment coefficient and the dynamic pitch damping sum ($C_{m_q} + C_{m_{\dot{\alpha}}}$) for the Basic Finner at $M_\infty = 1.96$ is presented in Fig. 5. The pitching-moment data computed with the static, steady-state flow solver and obtained from the DC component of the reduced-frequency method is compared against wind tunnel data[28]. The pitch damping sum is compared against wind tunnel[28] and range data[29], along with a general time-dependent simulation. The pitching moment calculated from the static, steady-state solver and the DC component are in excellent agreement. The agreement between the computations and the wind tunnel data is good at the higher angles of attack. Uselton et al.[28] note sting effects below $\alpha = 6°$ in the wind tunnel tests. Both the non-zero moment and the better agreement between the pitch-damping computations and the range data at $\alpha = 0°$ substantiates this observation. At $\alpha = 20°$ the wind tunnel pitching moment begins to decrease due to flow separation, while the Euler computations do not. This is consistent with the expected behavior of an inviscid simulation at high angles of attack. The reduced-frequency and time-dependent predictions of the pitch damping sum are in very good agreement, except at $\alpha = 20°$. At the higher angles of attack the non-linear fluid dynamic effects increase and the response to a forced oscillation can develop higher frequencies. These higher frequencies cannot be resolved with the reduced-frequency scheme. Given this, the reduced-frequency calculations are still in good agreement with the wind tunnel data at the higher angles of attack. The lower angles of attack are limited by the sting effects noted above.

In the forced oscillation technique for determining dynamic derivatives, the amplitude and frequency of the oscillation are chosen to provide an accurate estimate of the damping behavior at the flight conditions of interest. The sensitivity of the reduced-frequency method to the choice of the oscillation amplitude and frequency is presented in Fig. 6. The wind tunnel data was obtained with a pitch amplitude of 1° and an oscillation frequency of 50 Hz.

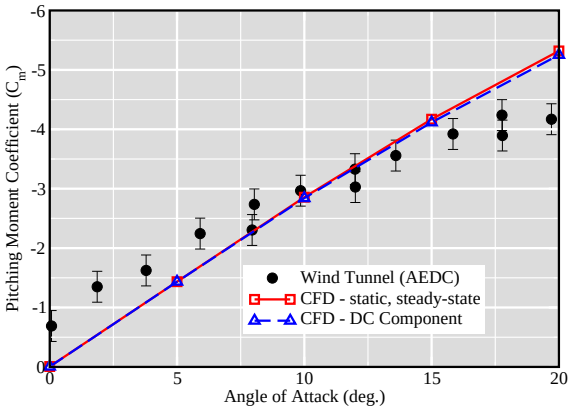

(a) Pitching Moment

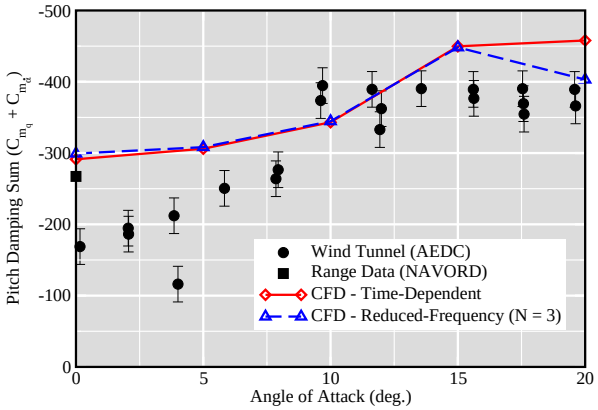

(b) Pitch Damping

Figure 5: Computed results for the pitch behavior of the Basic Finner configuration. Experimental data from [28] and [29]. ($M_\infty = 1.96$, $\phi = 45°$).

The reduced-frequency calculations are generally insensitive to amplitude and frequency variation at the lower angles of attack. As the angle of attack increases so do the non-linear fluid dynamic interactions, and the method is more sensitive to the choice of parameters. The smaller amplitude variation is preferred to provide an estimate of the damping derivative local to the flight condition of interest (cf. Uselton and Uselton[30]). Similarly, a high-frequency oscillation can potentially obscure the damping properties. An oscillation frequency of 50 Hz is used for the sub-scale models tested in this work, which roughly matches the frequency used in the corresponding wind tunnel testing.

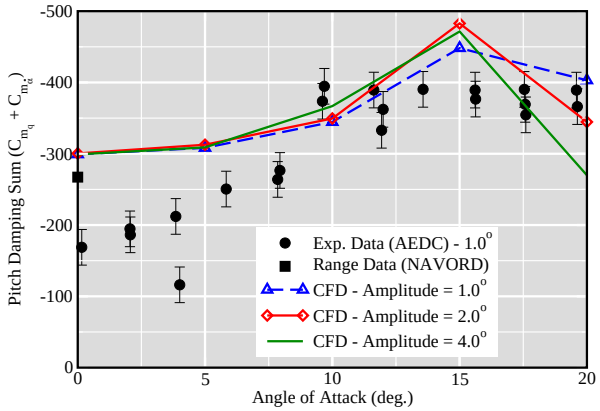

(a) Amplitude

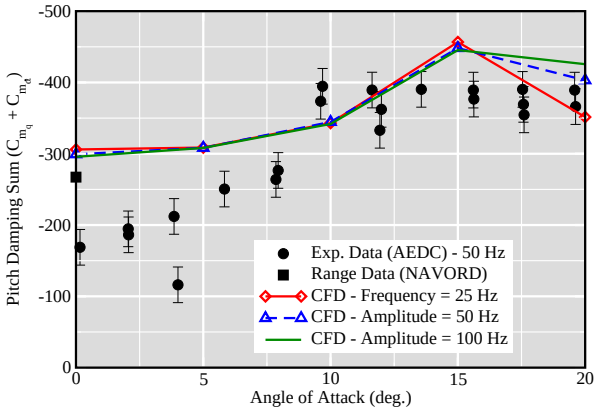

(b) Frequency

Figure 6: Sensitivity to input parameters for the forced-oscillation method. Experimental data from [28] and [29]. ($M_\infty = 1.96$, $\phi = 45°$).

4.2 Modified Basic Finner Missile

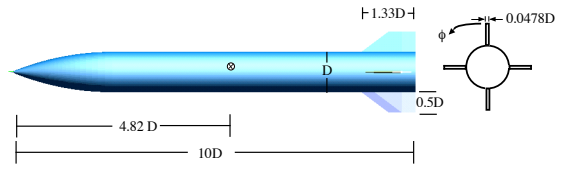

Figure 7: Modified Basic Finner geometry is a 2.5 calibar tangent-ogive cylinder fuselage with trapezoidal fins in the + configuration. The center of mass is located 4.82 diameters from the nose along the longitudinal axis of the body.

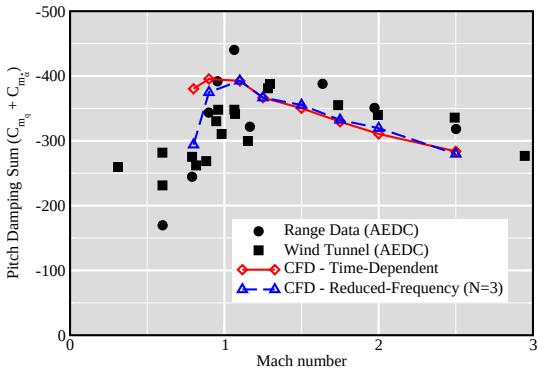

Figure 8: Variation of pitch damping with Mach number for the Modified Basic Finner. Experimental data from [31]. ($\alpha = 0°$, $\phi = 0°$).

The Modified Basic Finner configuration is a 2.5 calibar tangent-ogive cylinder forebody with 4 trapezoidal fins (cf. Fig. 7). The previous section presented the computed pitch-damping variation with angle of attack at supersonic conditions for the Basic Finner. A similar comparison is presented for the Modified Basic Finner in Fig. 8, this time holding the angle of attack fixed ($\alpha = 0°$) and varying the Mach number through the transonic range. Wind tunnel and range data[31] are included for validation of the reduced-frequency computations, along with computed results from a time-dependent scheme. The reduced-frequency calculations are in good agreement with the test data, capturing the rise in damping through Mach 1 along with the linear decay in the supersonic range. The reduced-frequency and time-dependent calculations are nearly identical except at $M_\infty = 0.8$, where high frequencies appear which cannot be resolved with the reduced-frequency method. The reduced-frequency method is, however, in better agreement with the test data at this Mach number indicating that these high frequencies are spurious, possibly generated from the blunt aft end.

4.3 Standard Dynamics Model Aircraft

The Standard Dynamics Model (SDM) is a test configuration designed loosely on the F-16 aircraft, including wing leading-edge extensions (LEX), horizontal and vertical stabilizers, ventral fins, a canopy, and an inlet section (cf. Fig. 9). Further details on the geometry of the configuration can be found in Beyers[32]. The computational resolution study resulted in a mesh with 2.6M cells. A cutting-plane through the lateral symmetry plane of the mesh, along with pressure contours is shown in Fig. 9. The SDM configuration has been tested extensively at various facilities and flight conditions. In the current work, variations of the damping coefficients through the transonic range at $\alpha = 0°$, and the variation with angle of attack

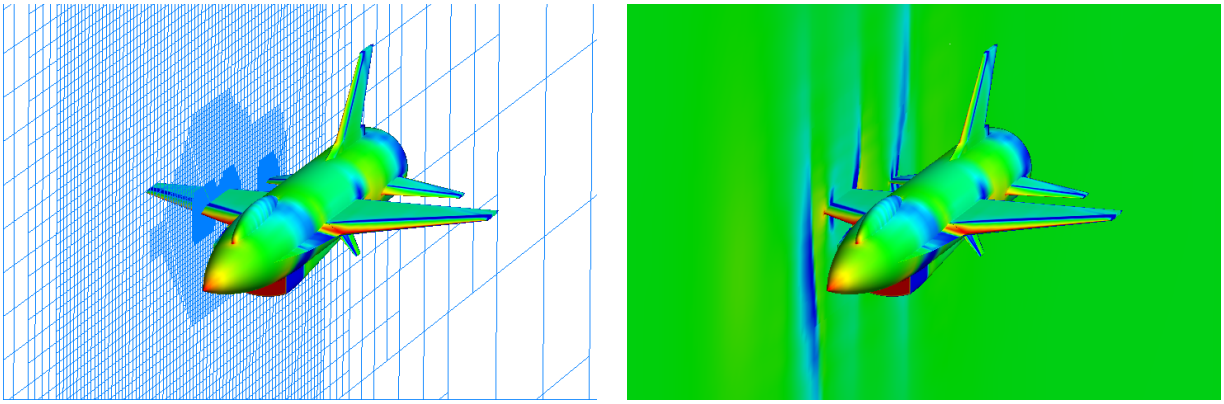

(a) Cutting plane through mesh (b) Pressure contours ($M_\infty = 0.95$, $\alpha = 0°$)

Figure 9: Standard Dynamics Model is a test configuration with trapezoidal wings and stabilizers, based loosely on the F-16 aircraft. Further information on the geometry can be found in Beyers[32].

at $M_\infty = 0.6$, are used to validate the reduced-frequency method. Comparisons against calculations using the time-dependent method are only included for the pitch-damping sum due to the high computational cost of the time-dependent method.

A complete set of damping derivatives for the SDM at $\alpha = 0°$ is compared against the wind tunnel and range data of Winchenbach et al.[33]. Figures 10-12 present the pitch, yaw, and roll damping through the transonic Mach number regime. For each damping derivative, the comparison between the reduced-frequency calculations and the test data is very good, with the increase in damping through Mach 1 clearly evident. Time-dependent simulation results are included for the pitch-damping calculations, and there is little difference between the reduced-frequency and time-dependent methods except near Mach 1. As with the Basic Finner and Modified Basic Finner, the results from the reduced-frequency simulations are in closer agreement with the available data than the time-dependent calculations.

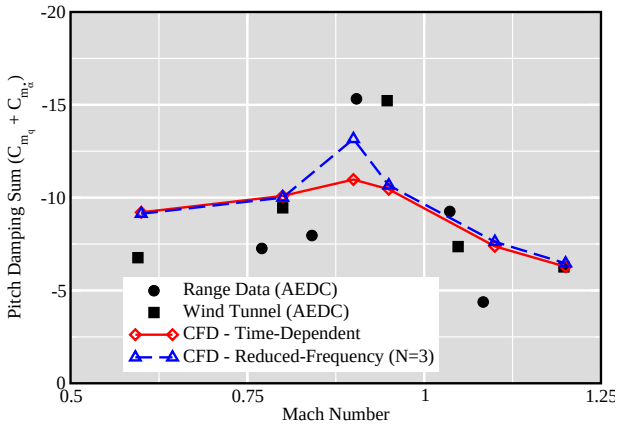

Figure 10: Variation of pitch damping with Mach number for the SDM at $\alpha = 0°$. Wind tunnel and range data from Winchenbach et al.[33]

The variation of pitch and roll damping with angle of attack for the SDM at Mach 0.6 is presented in Figs. 13 and 14. The computed results are compared against the wind tunnel data of Beyers[32, 34]. This case is especially interesting for the current validation as these are flight conditions which are expected to produce a wide energy-band response to a forced oscillation. The roll damping is essentially constant through the angle of attack range,

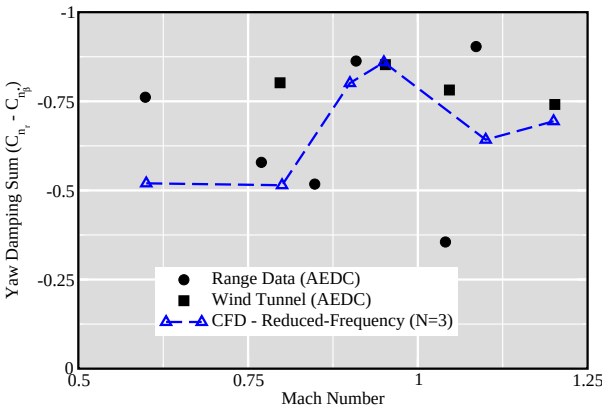

Figure 11: Variation of yaw damping with Mach number for the SDM at $\alpha = 0°$. Wind tunnel and range data from Winchenbach et al.[33]

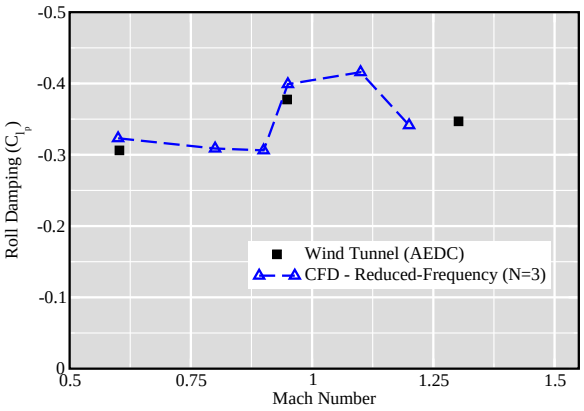

Figure 12: Variation of roll damping with Mach number for the SDM at $\alpha = 0°$. Wind tunnel data from Winchenbach et al.[33]

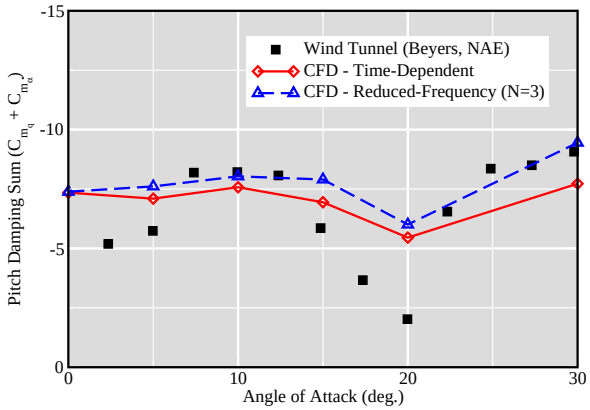

Figure 13: Variation of pitch damping with angle of attack for the SDM at Mach 0.6. Wind tunnel data from Beyers[34].

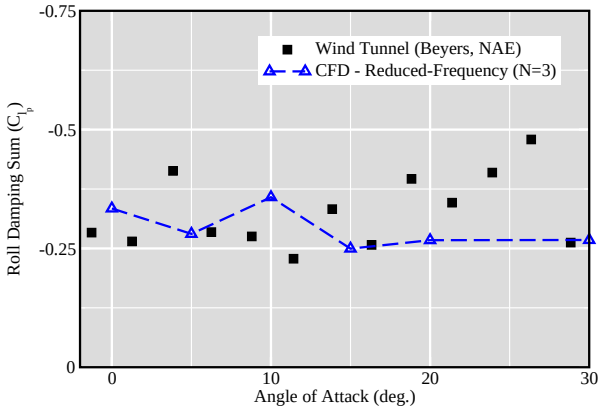

Figure 14: Variation of roll damping with angle of attack for the SDM at Mach 0.6. Wind tunnel data from Beyers[32].

and the reduced-frequency calculations predict this behavior. The comparison of the pitch damping with the wind tunnel data shows that the reduced-frequency calculations are in good agreement, but do underpredict the reduction in pitch damping at $\alpha = 20°$ due to the flow separation (as the angle of attack increases beyond $\alpha = 20°$ the LEX vortex lift increases the pitching damping). The time-dependent scheme is a slight improvement, indicating that the higher frequency modes being resolved are physical, but here the inviscid scheme cannot capture all aspects of the true viscous flow. It would be an interesting experiment to determine the performance of a Reynolds-averaged solver and turbulence model for these same flight conditions.

5 Summary and Future Work

A novel method of calculating dynamic stability derivatives using CFD methods has been presented. This method uses a non-linear, reduced-frequency approach to simulate the response to a forced oscillation using a single frequency component at the forcing frequency. This reduced-frequency approach was implemented with an automated Cartesian method, providing an efficient method for calculating damping derivatives under general flight conditions for a configuration of arbitrary complexity. The method was validated for reference missile and aircraft dynamic test configurations through the transonic and high-alpha flight regimes. The agreement between the simulations and the available wind-tunnel and ballistic-range data is very good. The reduced-frequency method provides nearly an order of magnitude improvement in computational efficiency over general time-dependent schemes.

The validation cases in this work do not include moving control surfaces, or inlet and exhaust conditions, both of which are required for an accurate analysis of a flight control system. Efficient methods of incorporating moving control surfaces with automated parameter studies using the current Cartesian approach have been demonstrated[21]. A method of simulating inlet and exhaust conditions has also been validated[35]. Along with the current work, this provides an automated, efficient infrastructure for determining the aerodynamic performance of a vehicle at flight operating conditions. With this aerodynamic database in hand, a preliminary design or mission analysis can quickly be evaluated. The development of novel control system concepts and optimization of controllers for specific mission requirements have already been demonstrated with this system[21].

The validation cases presented assume a linear damping model. The reduced-frequency approach will converge for conditions which lead to non-linear damping, however, it is currently not possible to discriminate between a calculation in the linear or non-linear damping regimes. It is not clear if it is appropriate to assume that a calculation with the reduced-frequency method, which assumes a linear damping modeled, is a linearized, leading-order approximation to the non-linear damping. Further research into calculating the response to non-linear damping with a reduced-frequency approach is warranted.

All of the dynamic derivative calculations presented use the forced-oscillation technique. Other experimental methods for determining the dynamic response of a configuration are the rotary-balance and body roll axis tests. These tests also produce periodic solutions, however in many cases the frequency is coupled to the geometry. For example, a missile with two canards and three tail fins will have two frequency components in a roll-axis simulation, while other geometric configurations will differ. This coupling makes it difficult to develop computational methods which are fully automated. Further, these types of tests often produce average coefficients, e.g. roll-averaged roll damping, as opposed to the point values produced with the forced-oscillation technique. Examining methods of incorporating general periodic motions with the reduced-frequency technique for calculating dynamic derivatives is thus left as a topic for future work.

Acknowledgments

I would like to thank Mike Aftosmis (NASA Ames), Marsha Berger (NYU), and Marian Nemec (ELORET) for their support and advice. This work was supported by NASA Ames Research Center (contract NAS2-00062).

References

[1] Cormier, J., Champagneux, S., Moreuxt, V., and Collercandy, R., "Prediction of Quasi-Stationary Aerodynamic Coefficients Using the ALE Method," in *ECCOMAS 2000*, (Barcelona, Spain), Sept. 2000.

[2] Pechier, M.., Guillen, P., and Cayzac, R., "Magnus Effect over Finned Projectiles," *Journal of Spacecraft and Rockets*, 38(4):542–549, July 2001.

[3] Oktay, E. and Akay, H. U., "CFD Predicitions of Dynamic Derivatives for Missiles," AIAA Paper 2002-0276, Jan. 2002.

[4] Park, S.H., Kim, Y., and Kwon, J.H., "Predicition of Dynamic Damping Coefficients Using the Unsteady Euler Equations," *Journal of Spacecraft and Rockets*, 40(3):356–362, 2003. Also AIAA Paper 2002-0715.

[5] Murman, S.M., Aftosmis, M.J., and Berger, M.J., "Numerical Simulation of Rolling-Airframes Using a Multi-Level Cartesian Method," *Journal of Spacecraft and Rockets*, 41(3):426–435, 2004. Also AIAA Paper 2002-2798.

[6] Schiff, L.B., "Nonlinear Aerodynamics of Bodies in Coning Motion," *AIAA Journal*, 10 (11):1517–1522, 1972.

[7] Weinacht, P., Sturek, W.B., and Schiff, L.B., "Navier-Stokes Predictions of Pitch-Damping for Axisymmetric Shell Using Steady Coning Motion," AIAA Paper 91-2855, Aug. 1991.

[8] Park, S.H. and Kwon, J.H., "Navier-Stokes Computations of Stability Derivatives for Symmetric Projectiles," AIAA Paper 2004-0014, Jan. 2004.

[9] Weinacht, P., "Navier-Stokes Predictions of the Individual Components of the Pitch-Damping Sum," *Journal of Spacecraft and Rockets*, 35(5):598–605, Oct. 1998.

[10] Weinacht, P. and Sturek, W., "Computations of the Roll Characteristics of a Finned Projectile," *Journal of Spacecraft and Rockets*, 33(6):769–775, Nov. 1996.

[11] Green, L., Spence, A.M., and Murphy, P.C., "Computational Methods for Dynamic Stability and Control Derivatives," AIAA Paper 2004-0015, Jan. 2004.

[12] Stalnaker, J., "Rapid Computation of Dynamic Stability Derivatives," AIAA Paper 2004-0210, Jan. 2004.

[13] Hall, K., Thomas, J., and Clark, W., "Computation of Unsteady Nonlinear Flows in Cascades Using a Harmonic Balance Technique," in *9th International Symposium on Unsteady Aerodyamics, Aeroacoustics, and Aeroelasticity of Turbomachines*, (Lyon, France), Sept. 2000.

[14] Hall, K., Thomas, J., and Clark, W., "Computation of Unsteady Nonlinear Flows in Cascades Using a Harmonic Balance Technique," *AIAA Journal*, 40(5):879–886, May 2002.

[15] McMullen, M., Jameson, A., and Alonso, J., "Acceleration of Convergence to a Periodic Steady State in Turbomachinery Flows," AIAA Paper 2001-0152, Jan. 2001.

[16] McMullen, M., Jameson, A., and Alonso, J., "Application of a Non-Linear Frequency Domain Solver to the Euler and Navier-Stokes Equations," AIAA Paper 2002-0120, Jan. 2002.

[17] Aftosmis, M.J., Berger, M.J., and Melton, J.E., "Robust and Efficient Cartesian Mesh Generation for Component-Based Geometry," *AIAA Journal*, 36(6):952–960, June 1998.

[18] Haimes, R. and Aftosmis, M.J., "On Generating High Quality "Water-tight" Triangulations Directly from CAD," in *Meeting of the International Society for Grid Generation (ISGG) 2002*, June 2002.

[19] Murman, S.M., Aftosmis, M.J., and Berger, M.J., "Implicit Approaches for Moving Boundaries in a 3-D Cartesian Method," AIAA Paper 2003-1119, Jan. 2003.

[20] Rogers, S. E., Aftosmis, M. J., Pandya, S. A., Chaderjian, N. M., Tejnil, E. T., and Ahmad, J. U., "Automated CFD Parameter Studies on Distributed Parallel Computers," AIAA Paper 2003-4229, June 2003.

[21] Murman, S.M., Aftosmis, M.J., and Nemec, M., "Automated Parameter Studies Using a Cartesian Method," AIAA Paper 2004-5076, Aug. 2004.

[22] Kalviste, J., "Use of Rotary Balance and Forced Oscillation Test Data in Six Degrees of Freedom Simulation," AIAA Paper 82-1364, 1982.

[23] O'Connor, C.J., Ralston, J.N., Fitzgerald, T., "Evaluation of the NAWC/AD F/A–18 C/D Simulation Including Database Coverage and Dynamic Data Implementation Techniques," AIAA Paper 96-3365, 1996.

[24] Brandon, J.M. and Foster, J.V., "Recent Dynamic Measurements and Considerations for Aerodynamic Modeling of Fighter Airplane Configurations," AIAA Paper 98-4447, 1998.

[25] Aftosmis, M.J., Berger, M.J., and Adomavicius, G., "A Parallel Multilevel Method for Adaptively Refined Cartesian Grids with Embedded Boundaries," AIAA Paper 2000-0808, Jan. 2000.

[26] Landon, R.H., "Compendium of Unsteady Aerodynamic Measurements," AGARD Report No. 702, Aug. 1982.

[27] Berger, M.J., Aftosmis, M.J., and Murman, S.M., "Linearity-Preserving Limiters on Irregular Grids," AIAA Paper 2005-0490, Jan. 2005.

[28] Uselton, B.L. and Uselton, J.C., "Test Mechanism for Measuring Pitch Damping Derivatives of Missile Configurations at High Angles of Attack," AEDC Technical Report AEDC-TR-75-43, May 1975.

[29] Shantz, I. and Graves, R.T., "Dynamic and Static Stability Measurements of the Basic Finner at Supersonic Speeds," NAVORD Report 4516, Sept. 1960.

[30] Uselton, J.C. and Uselton, B.L., "A Look at the Validity of the Small-Amplitude Oscillation Dynamic-Stability Measurement Technique," AIAA Paper 75-211, Jan. 1975.

[31] West, K.O and Whyte, R.H., "Free Flight and Wind Tunnel Test of a Missile Configuration at Subsonic and Transonic Mach Numbers with Angles of Attack up to 30 Degrees," in *11th Navy Symposium on Aeroballistics*, pp. 361–399.

[32] Beyers, M.E., "Subsonic Roll Oscillation Experiments on the Standard Dynamics Model," AIAA Paper 83-2134, 1983.

[33] Winchenbach, G.L., Uselton, B.L., Hathaway, W.H., and Chelekis, R.M., "Comparison of Free-Flight and Wind Tunnel Data for a Generic Fighter Configuration," AIAA Paper 82-1365, 1982.

[34] Beyers, M.E., "Direct Derivative Measurements in the Presence of Sting Plunging," AIAA Paper 84-2107, 1984.

[35] Pandya, S.A., Murman, S.M., and Aftosmis, M.J., "Validation of Inlet and Exhaust Boundary Conditions for a Cartesian Method," AIAA Paper 2004-4837, Aug. 2004.